Cut diagrams for high energy scatterings

Y. J. Feng,[*] O. Hamidi-Ravari,[†] and C. S. Lam[‡]

Department of Physics, McGill University, 3600 University St., Montreal, P.Q., Canada H3A 2T8

(Received 26 April 1996)

A new approach is introduced to study QCD amplitudes at high energy and comparatively small momentum transfer. Novel cut diagrams, representing the resummation of Feynman diagrams, are used to simplify the calculation and to avoid delicate cancellations encountered in the usual approach. An explicit calculation to the sixth order is carried out to demonstrate the advantage of cut diagrams over Feynman diagrams. [S0556-2821(96)02417-4]

I. INTRODUCTION

The rapidity-gap events recently observed at the DESY *ep* collider HERA [1] revived the community's interest in the Regge-pole description of high energy scattering. The word ''Pomeron,'' seldom heard in recent years, is once again found in the lexicon of experimentalists. It is perhaps then a good time to have a new look at the connection between perturbative QCD and the Regge pole. Nonperturbative effects may be important for a momentum transfer of the order of Λ_{QCD} or smaller, but we shall avoid it by going to a larger momentum transfer if necessary.

It was proposed by Low [2] and Nussinov [2] some years ago that the Pomeron may simply reflect a two-gluon exchange in QCD. Diagrammatic calculations have been carried out [3–8] in the leading-logarithmic approximation to substantiate this proposal and to study other aspects of the high energy near forward scattering amplitudes. We shall follow the classical approach of implementing physical (*s*-channel) unitarity by summing up Feynman diagrams in the Feynman gauge [3,4]. However, other approaches are available. The use of a physical gauge and dispersion relation [5] can sometimes make things more transparent. One can also emphasize the complex angular momentum aspect by concentrating on *t*-channel towers and their interactions as guided by *t*-channel unitarity [6]. We shall speak no further of these alternate approaches except to remark that our cut diagram method, to be discussed below, can be thought of as an intermediate link between the classical Feynman diagram sum and the dispersion relation approaches.

Because of the gauge and non-Abelian nature of the theory, perturbative calculations are lengthy and complicated. Even by ignoring self-energy and vertex corrections, as well as renormalization effects, on the grounds that they will not alter the qualitative nature of high energy scattering we are trying to learn, and even by ignoring quark pair productions as a first step, a complete QCD calculation can be carried out only up to sixth order. In the much simpler case of QED, an eighth order calculation [9] was reported to have taken 16 months and 2000 pages to complete. In the case of

QCD, it is much worse; a complete calculation of the eighth order is not available, though partial calculations have been carried out [7].

What makes the calculation so complicated is the large number of diagrams that have to be tackled, and the inevitable cancellations between them. The computation of each diagram is fairly straightforward, though somewhat lengthy at higher orders. After the individual diagrams are calculated, care must also be exercised to add them up because of the presence of many delicate cancellations. Leading-logarithmic dependences on energy get subtracted away, and complicated functions of momentum transfer also disappear. What emerges at the end is a product that is surprisingly simple. To the extent that it has been verified, high energy near forward scattering is described by multiple Reggeized gluon exchange, supplemented by elementary gluon production off the Reggeons and by *s*-channel unitarity [3,7].

This outcome has been verified up to sixth order [3–5]. As mentioned above, many delicate cancellations take place in the sum to enable this simple picture to emerge. A complete calculation in eighth order is not available, but if one assumes these cancellations which take place up to sixth order also occur in eighth and higher orders, then this Reggeized picture has been verified up to tenth order [7]. This gives strong support to the conjecture that it is true to all perturbative orders.

While the conjecture is attractive, it is impossible to verify or refute without a new method to simplify the complicated calculations. We report in this article such a new method, in which high energy scatterings are computed via *cut diagrams* rather than the normal Feynman diagrams. These cut diagrams are *not* the Cutkosky cut diagrams. The sum of all cut diagrams here is equal to the sum of all Feynman diagrams, and not just their discontinuities. These cut diagrams can be regarded as a resummation of the Feynman diagrams in which many of the delicate cancellations encountered in the latter have been built in and explicitly avoided. Consequently, the simplicity of the final sum is revealed already in individual cut diagrams, and not masked by terms to be canceled as is the case with Feynman diagrams. In addition, individual cut diagrams are easier to calculate than individual Feynman diagrams.

In this paper we shall introduce the formalism of cut diagrams, as well as an explict calculation to sixth order to demonstrate its effectiveness. We shall discuss quark-quark

_____

[*]Electronic address: feng@physics.mcgill.ca
[†]Electronic address: omid@physics.mcgill.ca
[‡]Electronic address: lam@physics.mcgill.ca
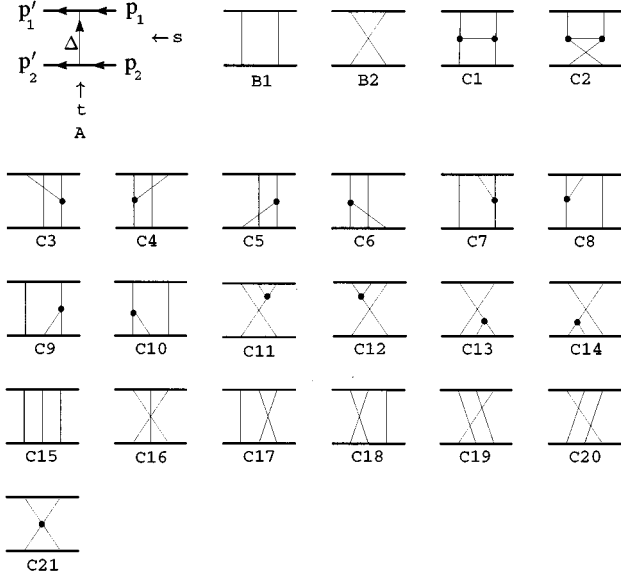
FIG. 1. Quark-quark scattering in QCD up to the sixth order. The thick lines at the top and bottom of each diagram are the fermion lines, and the thin lines are gluon lines.

scattering throughout but allow the quarks to carry any SU(N) color charge. The result should be equally valid for gluon-gluon and other scatterings because high energy processes are insensitive to the spins of the colliding particles [5,7,8]. This is so because the current carried by a high energy particle is dominated by its center-of-mass motion, with the spin current only an insignificant part of that. Formally, the two extra terms in a triple-gluon vertex is a factor $\Delta/\sqrt{s}$ down in comparison for transversely polarized gluons, where Δ is the momentum transfer and $\sqrt{s}$ is the center-of-mass energy of the process.

We will study pure SU(N) QCD and ignore the production of quark pairs. If one is bothered by considering quark-quark scattering while ignoring quark production, one can consider instead gluon-gluon scattering, and as mentioned above, the result would be the same.

In a subsequent paper [10] we shall use the cut diagrams to discuss the Reggeization conjecture in higher orders.

In Sec. II the result of Feynman diagram calculations to $O(g^6)$ is reviewed. How these diagrams combine to give a sum much simpler than the individuals will be discussed in some detail. In Sec. III, we begin to examine more carefully these cancellations by using sum rules. In Sec. IV, the method of cut diagrams is explained, and in Sec. V, this method is applied to fourth and sixth order calculations to demonstrate the savings effected by this method.

II. ELASTIC SCATTERING UP TO $O(g^6)$

Leading-logarithmic calculations in QCD, at high c.m. energy $\sqrt{s}$ and comparatively small momentum transfer $\sqrt{-t}=\sqrt{\Delta^2}$, are discussed, among others [13], by Cheng and Wu [3]. Citations to the original literature can also be located there. We review in this section the calculation of quark-quark scattering to sixth order done in this standard way.

The relevant Feynman diagrams are given in Fig. 1. The second order diagram is labeled A, the fourth order diagrams

labeled $B1$ and $B2$, and the sixth order diagrams $C1-C21$. This last labeling is identical [11] to the ones used in Fig. 12.7 of Ref. [3].

Under the interchange of the Mandelstam variables $s=(p_1+p_2)^2$ and $u=(p_1-p_2')^2$, the spacetime parts of these diagrams are either self-conjugate, or one goes into another. For example, $A\leftrightarrow A$, $B2\leftrightarrow B1$, $C2\leftrightarrow C1$, $C15\leftrightarrow C16$, $C17\leftrightarrow C19$, and $C18\leftrightarrow C20$, under $s\leftrightarrow u$.

Normalizing the Dirac spinors to $\bar{u}u=1$, and designating the fermion mass and gauge coupling constant as m and g, with $\beta=g^2/2\pi$, the T-matrix element $\mathcal{T}=(g^2s/2m^2)\mathcal{M}$ receives the following contributions from the individual diagrams to $\mathcal{M}$ [3,4,12]:

$$A=-I_1\cdot\mathbf{G}_1,$$

$$B1=-\beta\ln(se^{-\pi i})I_2\cdot\mathbf{G}_2,$$

$$B2=+\beta(\ln s)I_2\cdot(\mathbf{G}_2+c\mathbf{G}_1),$$

$$\overline{C1}=+\beta^2\ln^2(se^{-\pi i})[\tfrac{1}{2}\Delta^2I_2^2-J_2I_2]\cdot\mathbf{G}_3,$$

$$\overline{C2}=-\beta^2(\ln^2s)[\tfrac{1}{2}\Delta^2I_2^2-J_2I_2]\cdot(\mathbf{G}_3+c^2\mathbf{G}_1),$$

$$C3=+\beta^2\{\ln^2(se^{-\pi i})-\ln^2s\}\tfrac{1}{4}J_2I_2\cdot(\mathbf{G}_3-c\mathbf{G}_2)$$
$$=C4=C5=C6,$$

$$C7=-\beta^2\ln^2(se^{-\pi i})\tfrac{1}{4}J_2I_2\cdot(-c\mathbf{G}_2)$$
$$=C8=C9=C10,$$

$$C11=+\beta^2(\ln^2s)\tfrac{1}{4}J_2I_2\cdot(-c\mathbf{G}_2-c^2\mathbf{G}_1)$$
$$=C12=C13=C14,$$

$$C15=-\beta^2(\ln s)2J_3\cdot\mathbf{G}_4,$$

$$C16=-\beta^2(\ln s)2J_3\cdot(\mathbf{G}_4-\mathbf{G}_3+3c\mathbf{G}_2+c^2\mathbf{G}_1),$$

$$C17=+\beta^2(\ln s)(J_3+\pi iI_3)\cdot(\mathbf{G}_4+c\mathbf{G}_2)=C18,$$

$$C19=+\beta^2(\ln s)(J_3-\pi iI_3)\cdot(\mathbf{G}_4-\mathbf{G}_3+2c\mathbf{G}_2)$$
$$=C20. \tag{2.1}$$

Part of $C21$ has been combined with $C1$ to form $\overline{C1}$, and the remaining part of $C21$ has been combined with $C2$ to form $\overline{C2}$. Note that the result for different diagrams is consistent with their $s\leftrightarrow u$ character, under whose exchange the $\mathcal{T}$ amplitude responds with the swap $se^{-\pi i}\leftrightarrow s$. See Appendixes A and B for a brief discussion of how these amplitudes are computed.

The two-dimensional vector Δ in the transverse direction is the momentum transfer. The functions $J_n(\Delta)$ and $I_n(\Delta)$ are defined as

$$I_1(\Delta)=\frac{1}{\Delta^2},$$

$$I_n(\Delta) = \int \left(\prod_{i=1}^{n} \frac{d^2 q_{i\perp}}{(2\pi)^2} \frac{1}{q_{i\perp}^2} \right) (2\pi)^2 \delta^2 \left(\sum_{i=1}^{n} q_{i\perp} - \Delta \right),$$

$$J_2(\Delta) = \int \frac{d^2 q_\perp}{(2\pi)^2} \frac{1}{q_\perp^2},$$

$$J_3(\Delta) = \int \left(\prod_{i=1}^{3} \frac{d^2 q_{i\perp}}{(2\pi)^2} \frac{1}{q_{i\perp}^2} \right) \frac{q_{2\perp}^2}{q_{2\perp}^2 - q_{3\perp}^2} \left[\ln \frac{q_{2\perp}^2}{q_{3\perp}^2} \right]$$

$$\times (2\pi)^2 \delta^2 \left(\sum_{i=1}^{n} q_{i\perp} - \Delta \right). \qquad (2.2)$$

The functions I_2, I_3, J_2, and J_3 are denoted, respectively, by I, I_1, K, and I_2 in Ref. [3]. The infrared divergences of these integrals can be regulated by a mass, either put in by hand or via the Higgs mechanism. This regulation discussed in the literature [3–9] does not affect the following discussions, and so we shall ignore it. There is, however, also an ultra-violet divergence in the integral defining $J_2(\Delta)$, but it turns out that this function disappears in the *sum* of the sixth order diagrams, and so it causes no trouble either.

The factors $\mathbf{G}_i$ in Eqs. (2.1) are the color factors, with $c = N/2$ for SU(N) colors. As defined in [3], $\mathbf{G}_1$, $\mathbf{G}_2$, $\mathbf{G}_3$, and $\mathbf{G}_4$ are, respectively, the color factors for the diagrams A, $B1$, $C1$, and $C15$. They can be computed by an elegant graphical method [3] from the SU(N) commutation relation and identities

$$[t_a, t_b] = if_{abc}t_c, \quad f_{abc}f_{abd} = 2c\delta_{cd},$$

$$i^3 f_{adg}f_{bed}f_{cge} = cif_{abc}. \qquad (2.3)$$

Hence the combination of color factors $\mathbf{G}_i$ given in Eqs. (2.1) for the various diagrams remains valid whatever the color of the quark is, although $\mathbf{G}_i$ themselves would be different for different colors of the quark. See Appendix A for a brief discussion on the computation of the color factors.

The sum of all the terms in Eqs. (2.1), from A to $C20$, is

$$\mathcal{M} = -\frac{1}{\Delta^2} [1 - \bar{\alpha}\ln s + \tfrac{1}{2}\bar{\alpha}^2 \ln^2 s] \cdot \mathbf{G}_1$$

$$+ \tfrac{1}{2} g^2 i (I_2 - 2\beta c I_3 \ln s) \cdot \mathbf{G}_2$$

$$+ g^2 i \beta \ln s [I_3 - \tfrac{1}{2}\Delta^2 I_2^2] \cdot \mathbf{G}_3 + g^4 \tfrac{1}{6} I_3 \cdot \mathbf{G}_4, \qquad (2.4)$$

with

$$\bar{\alpha}(\Delta) \equiv \beta c \Delta^2 I_2(\Delta). \qquad (2.5)$$

It is important to note the various cancellations taking place to make the sum (2.4) vastly simpler than the individual terms appearing in Eqs. (2.1).

(1) In fourth order, the leading term proportional to $\ln s$ is canceled out between $B1$ and $B2$ in the color amplitude proportional to $\mathbf{G}_2$, though not in $\mathbf{G}_1$.

(2) In sixth order, the leading $\ln s$ contributions to $\mathbf{G}_4$ from $C15$ to $C20$ also add up to zero. The expressions given in Eqs. (2.1) are not accurate enough to deal with the subleading terms. The term in Eq. (2.4) proportional to $\mathbf{G}_4$ is obtained separately from the eikonal formula.

(3) As a result of these cancellations, the energy dependence and the SU(N) (or c) dependence of the $\mathbf{G}_1$ amplitude is $(g^2 c \ln s)^m$, and those of $\mathbf{G}_2$, $\mathbf{G}_3$, and $\mathbf{G}_4$ are, respectively, $g^2(g^2 c \ln s)^m$, $g^2(g^2 \ln s)^m$, and $g^4(g^2 c \ln s)^m$. These dependences can be summarized all at once by introducing a different notation for the color factors. We shall use the notation $\mathbf{F}_{i,j}$ to denote a color factor with i parallel vertical lines connecting the two fermions, and j parallel horizontal lines joining any two of the vertical gluon lines. We shall also write $\mathbf{F}_{i,0}$ simply as $\mathbf{F}_i$. The relations with the color factors $\mathbf{G}_i$ are $\mathbf{G}_1 = \mathbf{F}_1$, $\mathbf{G}_2 = \mathbf{F}_2$, $\mathbf{G}_3 = \mathbf{F}_{2,1}$, and $\mathbf{G}_4 = \mathbf{F}_3$. The g, c, and $\ln s$ dependences of $\mathbf{F}_{i,j}$ in Eq. (2.4) are then given by $g^{2(i-1)}(g^2 c \ln s)^m c^{-j}$ for a diagram of order $2(m+i)$. We shall refer to such dependences as *Regge like*, for the Reggeization of the scattering amplitude to be discussed later relies critically on this feature of the scattering amplitude. Note from Eqs. (2.1) that contributions from individual diagrams are not Regge like. Only the sum is.

(4) Simplification in transverse-momentum dependences also occurs in the sum. The simple integrals I_n survive, but the complicated integral J_3 and the divergent integral J_2 do not appear in the sum. This cancellation is highly nontrivial because both of them contribute different amounts to different color amplitudes.

(5) More specifically, the function $J_3(\Delta)$ appears in all the color amplitudes $\mathbf{G}_1$, $\mathbf{G}_2$, $\mathbf{G}_3$, and $\mathbf{G}_4$ in diagrams $C15$–$C20$. Those in $\mathbf{G}_2$, $\mathbf{G}_3$, and $\mathbf{G}_4$ actually get canceled out in the sum, but its presence in the $\mathbf{G}_1$ amplitude survives. However, since this term is of order $g^6 \ln s$, it is negligible compared to terms of order $g^6 \ln^2 s$ appearing in the $\mathbf{G}_1$ amplitudes of $\overline{C2}$ and $C11$ to $C14$; it can be ignored in the leading-logarithmic result displayed in Eq. (2.4).

(6) Also, $J_2(\Delta)$ appears in the color amplitudes $\mathbf{G}_1$, $\mathbf{G}_2$, and $\mathbf{G}_3$ in individual diagrams $C1$–$C14$ and all these appearances get canceled out.

As a result of these cancellations, $\mathcal{M}$ acquires a very simple interpretation in terms of Reggeized gluon exchanges. These exchanges are constructed in such a way to ensure s-channel unitarity [3,7].

Let us denote the Reggeon propagator by

$$R_1(\Delta, s) = \frac{1}{\Delta^2} \exp[-\bar{\alpha}(\Delta)\ln s]. \qquad (2.6)$$

This reduces to the (transverse part of the) ordinary propagator $I_1(\Delta) = \Delta^{-2}$ for small $g^2 c \ln s$. Similarly, let us denote the Reggeized version of $I_n(\Delta)$ by

$$R_n(\Delta, s) = \int \left(\prod_{i=1}^{n} \frac{d^2 q_{i\perp}}{(2\pi)^2} R_1(q_{i\perp}, s) \right)$$

$$\times (2\pi)^2 \delta^2 \left(\sum_{i=1}^{n} q_{i\perp} - \Delta \right), \qquad (2.7)$$

indicating the exchange of n Reggeons. Then to order g^6 in $\mathcal{T}$, we can write

$$\mathcal{M} = -R_1(\Delta, s) \cdot \mathbf{F}_1 + i\frac{g^2}{2!}[R_2(\Delta, s) \cdot \mathbf{F}_2 + R_{2,1}(\Delta, s) \cdot \mathbf{F}_{2,1}]$$

$$+ \frac{g^4}{3!} R_3(\Delta, s) \cdot \mathbf{F}_3. \qquad (2.8)$$

In other words, the $\mathbf{F}_1$, $\mathbf{F}_2$, $\mathbf{F}_{2,1}$, and $\mathbf{F}_3$ components looked precisely like diagrams A, $B1$, $C1$, and $C15$, respectively, but with the vertical gluons replaced by their Reggeized version whose propagators are given in Eq. (2.6), *and* with all longitudinal-momentum integrations omitted. To interpret it this way for $R_{2,1}\mathbf{F}_{2,1}$ we need to know the Lipatov-Dickinson vertex [8] describing how elementary gluons are produced and absorbed from the Reggeized gluons.

This remarkable simplicity and regularity led to the conjecture [3,7] that the Reggeized formula (2.8), suitably generalized, is the correct high energy limit to all perturbative orders. This conjecture is very difficult to verify on account of the shear complexity in higher order calculations. For QCD in eighth order it is simply not manageable without simplifying assumptions. If one assumes that all cancellations that occurred up to $O(g^6)$ will also occur in higher orders, the final result can be extracted from a *relatively* small set of diagrams; then, it is reported that this Reggeization conjecture is true to eighth and tenth orders [7]. Even so these calculations are so lengthy and complicated that to our knowledge the full details have never been published.

III. HIGH ENERGY KINEMATICS

We shall discuss in the next two sections a method of using *cut diagrams* to sum up the Feynman diagrams, a method in which most of the cancellations discussed in the last section are automatically built in. This simplification shortens the computations and makes it possible to study higher order diagrams. In this paper we shall discuss how it simplifies the calculations up to $O(g^6)$. In a subsequent paper [10] we shall discuss how it helps to verify part of the Reggeization conjecture to all orders. To prepare the groundwork for both, we discuss here the relevant kinematical features of high energy scattering which enables this new method to work.

We will assume the colliding beams in their c.m. system to be directed along the z direction. In light-cone coordinates $p_{\pm} = p^0 \pm p^3$, the components of a four-vector are labeled in the order $p^\mu = (p_+, p_-, p_\perp)$, with the two-dimensional vector $p_\perp$ lying in the transverse x-y plane. In this notation, the incoming fermion momenta are $p_1 = (\sqrt{s}, 0, 0)$ and $p_2 = (0, \sqrt{s}, 0)$, in which their mass m has been neglected. The outgoing fermion momenta are approximately given by $p_1' = (\sqrt{s}, 0, \Delta)$ and $p_2' = (0, \sqrt{s}, -\Delta)$. See Fig. 1.

Suppose n gluons are hooked up to the upper fermion line as shown in Fig. 2. The initial and final fermions are on shell but the gluons can be off shell, though with an amount of energy far less than $\sqrt{s}$. At high energy, the numerator of the propagator can be approximated by

$$\gamma p = 2m \sum_\lambda u_\lambda(p_1) \bar{u}_\lambda(p_1), \qquad (3.1)$$
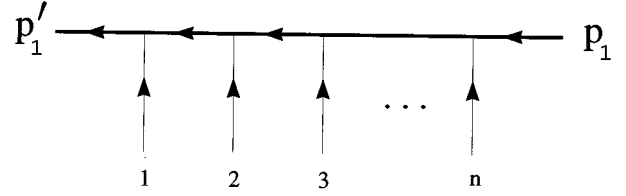
FIG. 2. A quark $\rightarrow$ quark $+ n$ gluon tree diagram.

provided the Dirac spinors are normalized to $\bar{u}_\lambda(p) u_{\lambda'}(p) = \delta_{\lambda\lambda'}$. With that, the dominant current $\bar{u}_\lambda(p_1) \gamma^\alpha u_{\lambda'}(p_1)$ at high energy is just its translational part $\delta_{\lambda\lambda'} p_1^\alpha / m$. This shows that the spin content at high energy is unimportant. All that it does is to enforce helicity conservation of the fermion, and to produce a factor $2p_1$ at each vertex together with an overall normalization factor of $1/2m$. For most of the discussions below we shall ignore this QED factor and concentrate on the contribution from the denominators, i.e., the corresponding scalar theory.

The denominator of the ith inverse propagator is

$$\left(p_1 + \sum_{j=1}^{i} q_j\right)^2 - m^2 + i\epsilon \simeq s\left(\sum_{j=1}^{i} x_j + i\epsilon\right), \qquad (3.2)$$

where $x_i = q_{i-}/\sqrt{s}$. The scalar amplitude in Fig. 2 is given by s^{-n} times

$$a[12\cdots n] \equiv -2\pi i \delta\left(\sum_{j=1}^{n} x_j\right) \prod_{i=1}^{n-1} \frac{1}{\Sigma_{j=1}^{i} x_j + i\epsilon}. \qquad (3.3)$$

Note that a momentum conservation δ function for the negative components (together with an explicit factor $-2\pi i$) has been incorporated. In Eq. (3.3) the ordering of the gluon lines from left to right is $[123\cdots n]$. If they are ordered differently, say, $[v_1 v_2 \cdots v_n] \equiv V$, then the corresponding amplitude is

$$a[v_1 v_2 \cdots v_n] \equiv a[V] \equiv -2\pi i \delta\left(\sum_{j=1}^{n} x_{v_j}\right)$$

$$\times \prod_{i=1}^{n-1} \frac{1}{\Sigma_{j=1}^{i} x_{v_j} + i\epsilon}. \qquad (3.4)$$

IV. SUM RULES

It is possible to compute sums of Feynman diagrams without much of the delicate cancellations discussed in Sec. II, by using the *cut diagrams* which we shall describe in this section and the next. The derivation of cut diagrams relies on two exact combinatorial formulas for the quantity $a[V]$ in Eq. (3.4): the *factorization formula* and the *multiple commutator formula* derived in Ref. [14]. We shall discuss the former in this section, and the latter in the next section.

Consider an ordering of n_i gluon lines: $[v_{i1} v_{i2} \cdots v_{in_i}] \equiv V_i$. We shall use the notation $\{V_1; V_2; \ldots; V_m\}$ to denote the *set* of *all* orderings of the $M \equiv \Sigma_{i=1}^{m} n_i$ gluon lines, *provided* the relative orderings of lines within each V_i are maintained. The number of orderings in this set is given by the multinominal coefficient
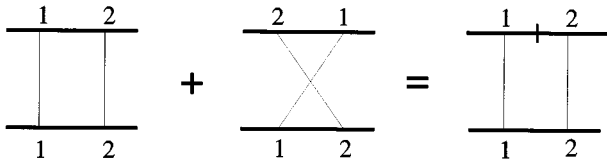
FIG. 3. An illustration of summing Feynman diagrams to obtain cut diagrams.

$M!/\Pi_{j=1}^{m} n_j!$. For example, if $V_1 = [135]$ and $V_2 = [24]$, then $\{V_1; V_2\} \equiv \{135; 24\}$ consists of the $5!/3!2! = 10$ orderings $[13524]$, $[13254]$, $[13245]$, $[12354]$, $[12345]$, $[12435]$, $[21354]$, $[21345]$, $[21435]$, and $[24135]$.

We shall use the notation

$$a\{V_1; V_2; \ldots; V_m\} = \sum_{V \in \{V_1; V_2; \cdots; V_m\}} a[V] \quad (4.1)$$

to denote the sum of all amplitudes for the gluon orderings in the set. The factorization formula [14] then states that

$$a\{V_1; V_2; \ldots, V_m\} = \prod_{i=1}^{m} a[V_i]. \quad (4.2)$$

In particular, if each set $V_i = [v_i]$ consists of only one gluon line labeled by v_i, then $\{V_1; V_2; \ldots; V_m\}$ is the set of *all* orderings of m gluon lines. In that case the factorization formula reduces to the well-known *eikonal formula* [3,15]. Other special cases of this formula have also been discovered before [7,16].

It is useful to adopt an alternative notation for the right-hand side of Eq. (4.2) to denote $\Pi_{i=1}^{m} a[V_i]$ simply as $a[V_1|V_2|\cdots|V_n]$. This notation is suggestive because the vertical bar can be interpreted graphically as a cut in the fermion propagator between the last gluon line of V_i and the first gluon line of V_{i+1}. For a cut propagator, instead of the usual factor $(\Sigma_{j=1}^{i} x_{v_j} + i\epsilon^{-1})$, we have $-2\pi i \delta(\Sigma_{j=1}^{i} x_{v_j})$. This notation is also convenient because it makes Eq. (4.2) deceptively simple. It now reads $a\{V_1; V_2; \ldots; V_m\} = a[V_1|V_2|\cdots|V_m]$; we simply have to change the semicolons to vertical bars.

Cut propagators are not limited to tree diagrams like Fig. 2. The off-shell gluons can be connected to other diagrams to form a composite diagram that inherits the original cuts. The cut diagrams so formed are similar to but different from the Cutkosky cut diagrams, similar because we have the same factors for the cut propagators, different because the cuts here occur only on fermion lines whereas in a Cutkosky diagram they can occur on any line. Moreover, via Eq. (4.2), our cut diagram represents a sum of $M!/\Pi_{j=1}^{m} n_j!$ (uncut) Feynman diagrams, with their real and imaginary parts fully

included, which is unlike the Cutkosky diagrams in which only the imaginary part or the discontiuity is represented.

It is clear from Eq. (4.2) that the factorization formula can be thought of as a sum rule to represent sums of Feynman diagrams as cut diagrams. As will be discussed in Appendix B, a cut diagram is easier to compute than an uncut diagram. In this way not only is it unnecessary to compute the individual diagrams first, the cut diagram representing the sum is actually easier to compute than just one single Feynman diagram.

We shall now apply the factorization formula to compute sums of amplitudes quoted in Sec. II. We shall see that the $\ln s$ factor and the J_i functions that get canceled out in the sum never once appear in the cut diagrams.

In what follows we shall use the notation $\langle B1 \rangle$ to denote the spacetime part of $B1$ (without the color factor $\mathbf{G}_2$). Similar notation will be used for the spacetime part of other diagrams as well.

In fourth order, the $\mathbf{G}_2$ coefficient in $\mathcal{M}$ is given by $\langle B1 \rangle + \langle B2 \rangle$. Using the eikonal formula $a[12] + a[21] = a[1|2]$ on the upper fermion line (see Fig. 3), $\langle B1 \rangle + \langle B2 \rangle$ is reduced to a cut diagram that can be easily calculated (see Appendix B for all the calculations), yielding the correct result $g^2 i I_2/2$ given in Eqs. (2.1) and (2.4). Similary, the sum rule $a\{1; 2; 3\} = a[1|2|3]$ applied to the six horizontal ladder diagrams in sixth order yields a cut diagram (see Fig. 4) which gives the sum of $\langle C15 \rangle - \langle C20 \rangle$ to be $g^4 I_3/6$. This is the correct coefficient of $\mathbf{G}_4$ given in Eq. (2.4). Note that neither $\ln s$ nor J_3 ever appears.

Let us now look at the cancellation of $J_3(\Delta)$ in the $\mathbf{G}_2$ and $\mathbf{G}_3$ color factors, as discussed in point (5) of Sec. II. According to Eqs. (2.1), the coefficient of $-\mathbf{G}_3$ from diagrams $C15-C20$ is given by $\langle C16 \rangle + \langle C19 \rangle + \langle C20 \rangle$. Using $a\{31; 2\} = a[31|2]$ on the upper fermion line as in Fig. 5, this sum is given by a cut diagram which can be evaluated to be $-g^4 i \ln s I_3/2\pi$. Again J_3 does not appear in the cut diagram. Similarly, the coefficient of $c\mathbf{G}_2$ from diagrams $C15-C20$ is given by Eqs. (2.1) to be $3\langle C16 \rangle + \langle C17 \rangle + \langle C18 \rangle + 2\langle C19 \rangle + 2\langle C20 \rangle$. This is equal to twice the previous sum, plus $\langle C16 \rangle + \langle C17 \rangle + \langle C18 \rangle$. To use the sum rule, this requires an expression (see Fig. 6) for $a[321] + a[213] + a[132]$. It is easy to see that this is equal to $a\{21; 3\} - a\{23; 1\} + a\{13; 2\}$ and, by the factorization formula, also equal to $a[21|3] - a[23|1] + a[13|2]$. There may seem to be very little gained by replacing the sum of three terms by the sum of another three terms, but this is not so. We are replacing the sum of three uncut diagrams by the sum of three cut diagrams. The computation of cut diagrams is much easier than the computation of uncut diagrams. For one thing the complicated function J_3 that appears on all three uncut diagrams but disappears from their sum never appears in any of the three cut diagrams. Evaluating the cut
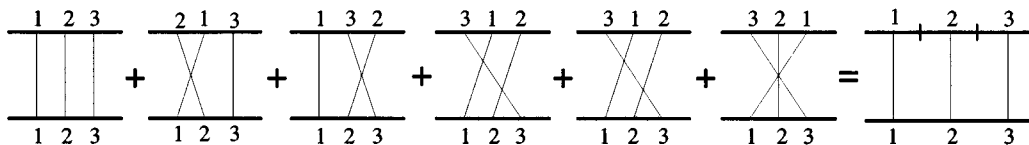
FIG. 4. Another sum rule.
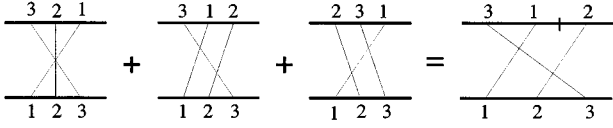
FIG. 5. Yet another sum rule.

diagrams, the coefficient of $c\mathbf{G}_2$ from $C15-C20$ is $-g^4 ic\ln s I_3/2\pi$, agreeing with the answer given in Eq. (2.4).

V. CUT DIAGRAMS

The method introduced in the last section has a serious shortcoming. It does not tell us which cut diagrams to compute without detailed considerations of the kind carried out there. In this section we discuss a remedy for this shortcoming with the help of the *multiple commutator formula* [12].

So far we have been treating Fig. 2 mostly as a QED or a scalar amplitude. For QCD the non-Abelian color matrices t_a have to be incorporated. Instead of Eq. (3.4) the amplitude is now

$$A[v_1 v_2 \cdots v_n] = a[v_1 v_2 \cdots v_n] t[v_1 v_2 \cdots v_n]$$
$$\equiv a[V] t[V] \equiv A[V], \qquad (5.1)$$

where $t[V] = t_{v_1} t_{v_2} \cdots t_{v_n}$. What we want is a formula for the sum of the $n!$ permuted gluon orderings, $\mathcal{A} = \Sigma_{V \in S_n} A[V]$. For QED, where we can take all $t_a = 1$, this is simply the eikonal formula, and so what we need is the non-Abelian generalization of it. This is the multiple commutator formula

$$\mathcal{A} \equiv \sum_{V \in S_n} a[V] t[V] = \sum_{V \in S_n} a[V_c] t[V_c']. \qquad (5.2)$$

It expresses the sum of $a[V] t[V]$ in terms of sums over the corresponding cut amplitude $a[V_c] t[V_c']$. Compared to the eikonal formula this looks complicated; instead of a single term on the right-hand side, we have now a sum over $n!$ terms. The complication is inevitable because we are attempting to sum up amplitudes for *every* color. However, we shall see that many of these terms are actually zero, and moreover, the cut diagrams on the right are considerably simpler to evaluate than the uncut diagrams on the left. Again delicate cancellations will largely be avoided as before.

What remains to be described is what the cut diagram V_c that corresponds to the Feynman diagram V is, as well as what the amplitudes $a[V_c]$ and $t[V_c']$ are. Given a $V = [v_1 v_2 \cdots v_n]$, start from the rightmost number v_n and proceed leftward until one comes to the first number less than v_n. Put a cut just to the right of this number. Then start from this number and proceed leftward again until one

comes to the first number that is less than this number, and another cut is put just to the right of this new minimum number. Continue this way until the end and we have constructed the cut diagram V_c. For example, for $n=2$, the two cut diagrams are $[12]_c = [1|2]$ and $[21]_c = [21]$. For $n=3$, the six cut diagrams are $[123]_c = [1|2|3]$, $[213]_c = [21|3]$, $[312]_c = [31|2]$, $[132]_c = [1|32]$, $[231]_c = [231]$, and $[321]_c = [321]$.

To each cut diagram we associate a spacetime cut amplitude $a[V_c]$ as described in the last section. Namely, it is given by Eq. (3.4) except the propagator at a cut is replaced by $-2\pi i \delta(\Sigma_j x_{v_j})$.

The complementary diagram V_c' of a cut diagram V_c is obtained as follows. If a cut appears between two numbers in V_c, then there will be no cut between the same two numbers in V_c', and vice versa. For $n=2$, the complementary cut diagrams are $[1|2]' = [12]$ and $[21]' = [2|1]$. For $n=3$, the complementary cut diagrams are $[1|2|3]' = [123]$, $[21|3]' = [2|13]$, $[31|2]' = [3|12]$, $[1|32]' = [13|2]$, $[231]' = [2|3|1]$, and $[321]' = [3|2|1]$.

When no cut appears in V_c' the color factor $t[V_c']$ is simply $t[v_1 v_2 \cdots v_n] = t_{v_1} t_{v_2} \cdots t_{v_n}$. If a cut appears between v_i and v_{i+1}, then the product $t_{v_i} t_{v_{i+1}}$ is replaced by their commutators $[t_{v_i}, t_{v_{i+1}}]$. If two or more consecutive cuts appear, then the corresponding product of t's is replaced by multiple commutators. For example, $t[2|13] = [t_2, t_1] t_3$, $t[2|3|1] = [t_2, [t_3, t_1]]$, and $t[4|3|2|15] = [t_4, [t_3, [t_2, t_1]]] t_5$.

VI. CUT AMPLITUDES TO $O(g^6)$

We shall compute the cut diagrams to $O(g^6)$ to demonstrate the simplifications obtained therefrom.

Using Eq. (5.2) on the upper fermion, we obtain a set of cut diagrams as shown in Fig. 7. This set is not unique as others can be obtained from a different labeling of the gluon lines.

In the horizontal ladder diagrams $B1$, $B2$, $C15-C20$, we choose the planar diagrams $B1$ and $C15$ to be the ones whose upper lines are completely cut. This fixes the labelling [12] for $B1$ and [123] for $C15$ as shown, and it in turn determines how diagrams $B2$ and $C16-C20$ are to be cut. Using computational methods discussed in Appendixes A and B, these diagrams yield

$$B1_c = +\tfrac{1}{2} g^2 i I_2 \cdot \mathbf{G}_2,$$

$$B2_c = +\beta(\ln s) I_2 \cdot c\mathbf{G}_1,$$

$$C15_c = +g^4 \tfrac{1}{6} I_3 \cdot \mathbf{G}_4,$$
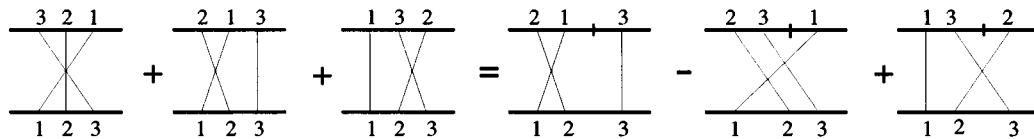
FIG. 6. An illustration of how sum of Feynman diagrams can be turned into a sum of cut diagrams.
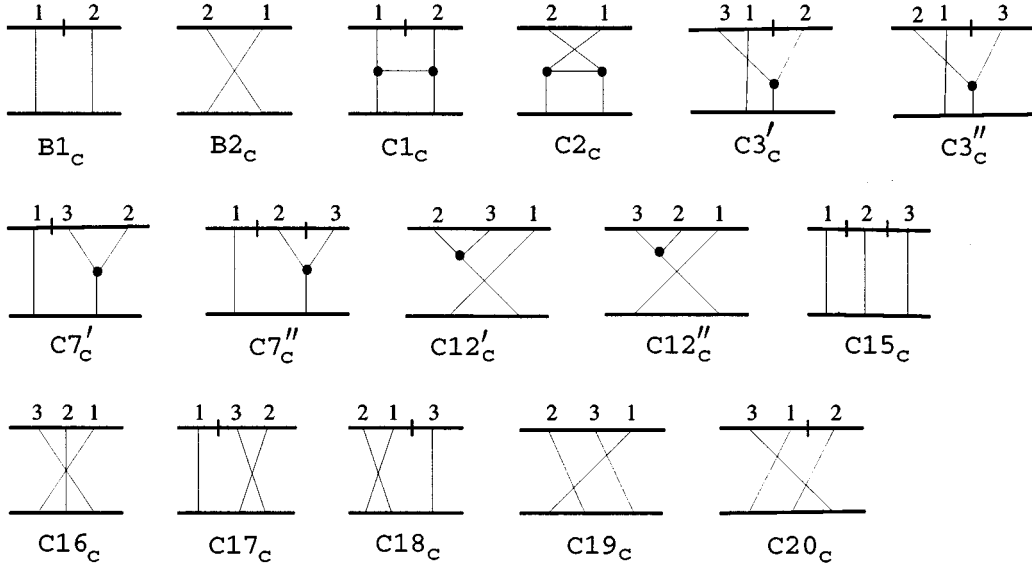
FIG. 7. Cut diagrams up to sixth order.

$$C16_c = -\beta^2(\ln s)2J_3 \cdot c^2\mathbf{G}_1,$$

$$C17_c = C18_c = 0,$$

$$C19_c = 0,$$

$$C20_c = -g^2\beta i(\ln s)I_3 \cdot (c\mathbf{G}_2 - \mathbf{G}_3). \qquad (6.1)$$

Similarly, we choose to cut the line of the planar diagram $C1$ to obtain

$$\overline{C1}_c = -g^2\beta i(\ln s)[\tfrac{1}{2}\Delta^2 I_2^2 - J_2 I_2] \cdot \mathbf{G}_3,$$

$$\overline{C2}_c = -\beta^2(\ln^2 s)[\tfrac{1}{2}\Delta^2 I_2^2 - J_2 I_2] \cdot c^2\mathbf{G}_1 \qquad (6.2)$$

The 12 diagrams $C3-C14$ can be divided into four groups of three, each giving identical contributions, and so it is necessary to consider only one of these groups. The group of $C3$, $C7$, $C12$ has been chosen for that purpose. There is a symmetry between gluon lines 2 and 3, and so we may double this group and consider it as a sum of six Feynman diagrams. By applying the multiple commutator formula, the six cut diagrams shown in Fig. 7 are obtained. Their values are

$$C3_c = \tfrac{1}{2}(C3'_c + C3''_c) = -g^2\beta i(\ln s)\tfrac{1}{4}J_2 I_2 \cdot \mathbf{G}_3,$$

$$C7_c = \tfrac{1}{2}(C7'_c + C7''_c) = 0,$$

$$C12_c = \tfrac{1}{2}(C12'_c + C12''_c) = \beta^2(\ln^2 s)\tfrac{1}{4}J_2 I_2 \cdot (-c^2\mathbf{G}_1).$$
$$(6.3)$$

The expressions in Eqs. (6.1)–(6.3) should be compared with those of the uncut diagrams, Eq. (2.1). It should also be compared with the sum found in Eq. (2.4). Several points can be noted from these comparisons:

(1) $\ln s$ factors that get canceled in the sum of the Feynman amplitude [see points (1)–(3) in Sec. II) never even appear in Eqs. (6.1)–(6.3). Cancellation of this kind is automatically built into the cut diagram formalism.

(2) The tranverse function J_3 appears only in $C16_c$ in Eq. (6.1). This expression survives the sum but can be ignored compared to the contribution from $\overline{C2}_c$. In other words, as opposed to the Feynman amplitude (2.1) where J_3 appears in many places but most of them are canceled out at the end [see points (4) and (5) in Sec. II], in the cut amplitude J_3 does not appear except when it survives the sum.

(3) The cut amplitude is not as successful in canceling the transverse function J_2 [point (6) of Sec. II], although there is still an improvement here over Eqs. (2.1) in that J_2 appears in fewer places. In fact, it appears in $C3_c-C20_c$ only when absolutely needed to cancel its previous appearance in $\overline{C1}_c$ and $\overline{C2}_c$. In order for J_2 to disappear completely it is necessary to combine diagrams with triple and four gluon vertices together using the Lipatov-Dickinson vertex [8]. The technique of cut diagrams by itself, which deals mainly with the fermion lines, is not sufficient for that purpose.

(4) Other than the J_2 complication mentioned above, the summands of the final answer (2.4) appear directly in the cut amplitudes. In that sense the cut amplitudes are as economical and as simple as they can ever be. In particular, the Regge-like feature mentioned in point (3) of Sec. II is present already in individual cut diagrams.

APPENDIX A: COLOR FACTORS

The method to compute the color factors graphically [3] is briefly reviewed here. It is suitable for both cut and uncut diagrams.
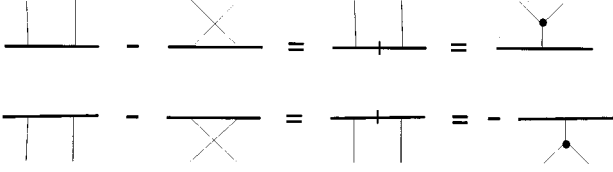
FIG. 8. Graphical represension of the commutation relation of color matrices. Thick lines are fermions and thin lines are gluons. The color factor at a gluon-fermion vertex is t_a of Eq. (2.3), and the color factor for a triple gluon vertex whose color indices a,b,c in the diagram are in clockwise order is if_{abc}. A cut represents a commutator between two color matrices.

The basic tool is the graphical identities depicted in Figs. 8 and 9, which are nothing but the commutation relation and identities in Eqs. (2.3). The commutation relation is valid for all representations of the color matrix t_a; hence, Fig. 8 remains true when the quark line is replaced by a gluon line.

As an example, the computation of the color factor for the uncut diagram $C19$ in Eq. (2.1) is carried out in Fig. 10, and the computation of the color factor for the cut diagram $C19_c$ in Eq. (6.1) is carried out in Fig. 11. For the latter, we have to remember to use the *complementary* cut diagram for the color factor, and not the cut diagram itself shown in Fig. 7.

The color factors in Eqs. (2.1), (6.1)–(6.3) can all be obtained in this way.

APPENDIX B: SPACETIME AMPLITUDES

The high energy limit of a Feynman diagram can be computed either in the Feynman-parameter representation [13] or directly in momentum space using light-cone coordinates [3–5]. We follow the latter approach and review briefly the main points. For a more detailed discussion see Ref. [3]. It serves well to remember at this point that the bottom fermion carries mostly the "$-$" momentum and the top fermion line carries mostly the "$+$" momentum.

The procedure to follow for the computation is simple: (i) Carry out the "$+$" momentum integration using residue calculus; (ii) then carry out the "$-$" momentum integration to produce the ln$s$ dependence. The transverse momentum integrations are never explicitly carried out, which is why the answers are all expressed in terms of functions like $I_n(\Delta)$ and $J_n(\Delta)$ given in Eq. (2.2).

Step (i) requires a knowledge of the location of poles for each propagator, which in turn depends on the choice of loop momenta k_a. Suppose $q = P + \Sigma_{a=1}^{\ell} c_a k_a$ is the momentum flowing through a propagator, with P being some combination of external momenta and c_a some integer coefficients.
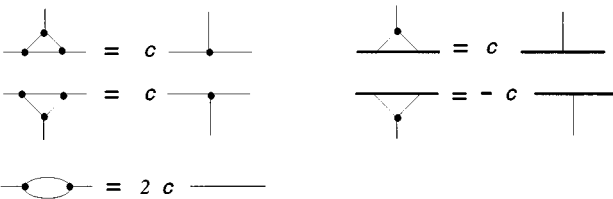
FIG. 9. Graphical represension of the last two identities in Eq. (2.3). $c = N/2$ for SU(N) color.
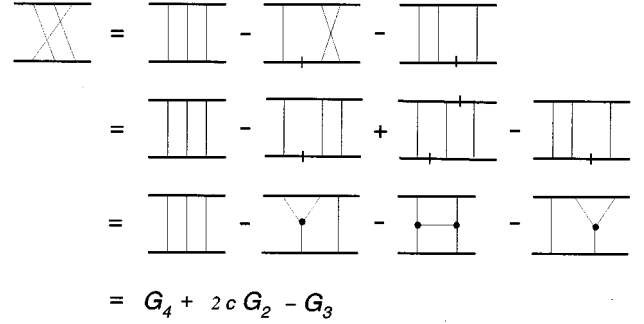
FIG. 10. A sample calculation of the color factor of a Feynman diagram.

The propagator $D^{-1} = (q^2 - m^2 + i\epsilon)^{-1} = (q_- q_+ - q_\perp^2 - m^2 + i\epsilon)^{-1}$ has a pole in the integration variable k_{a+} if $c_a \neq 0$. This pole is located in the upper half plane if $c_a q_-$ is negative, and in the lower half plane if it is positive. A way to keep track of the sign is to draw a *flow diagram* for the "$-$" momentum, with arrows indicating the direction of the "$-$" flow. See Fig. 12 for some illustrative examples. The arrows around a loop pointing one way (clockwise or counterclockwise) have their poles in one half plane, and those pointing the other way have poles in the opposite half plane. The arrows in the flow diagrams must obey momentum conservation, and one may also assume they do not go around in closed loops. Otherwise the poles will all be in the same half plane, and the integral is zero if the contour is closed in the opposite half plane. With these constraints we see in Fig. 12 that a one-loop diagram allows only one flow path, but for two and more loops there is bound to be more than one flow diagram because these constraints simply cannot fix the direction of the "$-$" flow on a boundary line of two loops.

Each flow diagram corresponds to a range of k_{a-} variables. By definition, the "$-$" variables along the direction of the flow are always non-negative.

We shall always close integration contours in the lower half planes, and indicate the poles so enclosed by a cross ($\times$) in the flow diagram. For a *scalar* diagram, the $\mathcal{T}$-matrix element is equal to the product of I propagators $D^{-1} = (q^2 - m^2 + i\epsilon)^{-1}$, integrated over the ℓ-loop momenta $d^4 k_a = \frac{1}{2} dk_+ dk_- d^2 k_\perp$, with an extra numerical factor $-[i/(2\pi)^4]^\ell$. Each "$+$" integration produces a factor $-2\pi i$; the $\mathcal{T}$ matrix is equal to

$$\mathcal{T} = -\sum \int Dk_\perp \left(\prod_{a=1}^{\ell} \frac{dx_a}{4\pi} \right) \frac{1}{\Pi_{i=1}^{I} D_i}, \qquad (B1)$$
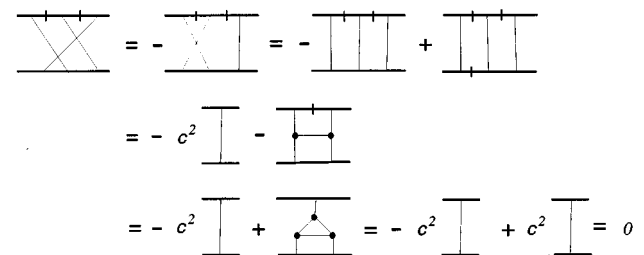
FIG. 11. A sample calculation of the color factor of a cut diagram.
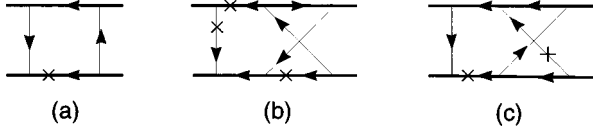
FIG. 12. Flow diagrams.

where $x_a = k_{a-}/\sqrt{s}$ is the scaled "$-$" momenta,

$$Dk_\perp \equiv \prod_{a=1}^{\ell} \frac{d^2 k_{a\perp}}{(2\pi)^2} \qquad (B2)$$

is the measure for transverse momentum integration, and D_i is either the propagator evaluated at the $\times$ poles or the residue of the $\times$ pole divided by $\sqrt{s}$. Each summand in Eq. (B1) corresponds to a flow diagram with a pole taken from the lower half plane (an $\times$ pole) of each loop. A flow diagram may have more than one set of $\times$ poles, in which case the sum is taken over all possible sets. For example, the one-loop diagram $B1$ in Fig. 1 has only one flow path [Fig. 12(a)] and one set of $\times$ poles. The two-loop diagram $C17$ of Fig. 1 has two flow paths, Figs. 12(b) and 12(c). The first flow diagram has two sets of $\times$ poles, and the latter flow diagram has one set of $\times$ poles. We shall see later that in the leading-logarithmic approximation, we may discard the q_+ dependence on the upper fermion line and the accompanied poles, in which case Fig. 12(b) is also left with one set of $\times$ poles.

Equation (B1) is also valid for cut diagrams, provided the propagator factor $D^{-1} = (q^2 - m^2 + i\epsilon)^{-1}$ of a cut line is replaced by $-2\pi i \delta(q^2 - m^2)$.

Let $q_{i-} = \sqrt{s} z_i$, $i = 1, 2, \ldots, I$. Every z_i is a linear combination of x_a, and in the case of a propagator along the bottom fermion line, $x_0 \equiv 1$ is also involved. The sign of each z_i is fixed by the direction of arrows in the flow diagram. If there are χ cut lines, then the last χ x_a will be chosen to be equal to $|z_i|$ of these cut lines. The I indices i will now be divided into three sets, a, b for indices from 1 to ℓ labeling the internal lines with an $\times$ pole, u for indices labeling propagators on the top fermion line, and m for the rest. Then $q_{a+} = q_{a\perp}^2/\sqrt{s} z_a$ and q_{m+}, q_{u+} can be expressed as linear combinations of q_{a+}: e.g.,

$$q_{m+} = \sum_a c_{ma} q_{a+} = z_m \sum_b c_{mb} q_{b\perp}^2/z_b. \qquad (B3)$$

Within the leading-logarithmic approximation, one has

$$D_a = z_a,$$

$$D_u \simeq s z_u \text{(uncut)}, \qquad D_u = -2\pi i \delta(s z_u) \text{(cut)},$$

$$D_m = \sum_b c_{mb} \frac{z_m}{z_b} q_{b\perp}^2 - q_{m\perp}^2 + i\epsilon. \qquad (B4)$$

The "$-$" momentum flows mainly along the bottom fermion line, with very little seeping out to avoid a substantial mixing with the "$+$" momentum coming from the top fermion line, for a finite mixture of these two at a propagator would make it proportional to s and therefore negligible.

This means that the dominant contribution to $\mathcal{T}$ comes from regions where all x_a are small. Since $x_a = 0$ for $a = \ell - \chi + 1, \ldots, \ell$, on account of the δ functions of the cut lines, the region of "$-$" integration can be roughly divided into regions where the remaining ($\ell' = \ell - \chi$ x_a)'s are strongly ordered, and regions where two or more of these x_a's are of the same order of magnitude. We shall label any one of the latter regions by S, and the former regions by $R[12\cdots\ell'] = \{1 \gg x_1 \gg x_2 \gg \cdots \gg x'_{\ell} \gg a/s\}$ and its permutations.

The x dependence of $\Pi_i D_i$ in $R[12\cdots\ell']$ is of the form $\Pi_{a=1}^{\ell'} x_a^{-m_a}$ and so the x integral encountered in Eq. (B1) is

$$\int_{\frac{a}{s}}^{x_{\ell'}} \frac{dx_{\ell'}}{x_{\ell'}^{m_{\ell'}}} \int_{x_{\ell'}} \frac{dx_{\ell'-1}}{x_{\ell'-1}^{m_{\ell'-1}}} \cdots \int_{x_2} \frac{dx_1}{x_1^{m_1}} \sim s^M (\ln s)^B, \qquad (B5)$$

where $M = \Sigma_{a=1}^{\ell'}(m_a - 1)$ and B is determined by how many times the sum $\Sigma_{a=1}^b (m_a - 1)$ reaches zero by varying b from 1 to ℓ'. Clearly $B \leq \ell'$, and the only way for $B = \ell'$ is to have all $m_a = 1$, in which case we will call the $\ln s$ dependence of $\mathcal{T}$ saturated. Otherwise it is said to be unsaturated. For the uncut diagrams, $\chi = 0$ and $\ell' = \ell$. We see in Eqs. (2.1) that all the diagrams except for the sixth order horizontal ladder diagrams $C15 - C20$ are saturated. For the cut diagrams in Eqs. (6.1)–(6.3), only $C16_c$ is unsaturated, but this diagram does not contribute to the final sum because of its subdominance.

The integral in an S region is like one in an R region with ℓ' reduced. For example, suppose $x_{\ell'-2}$ to $x_{\ell'}$ are roughly equal but x_1 to $x_{\ell''}$ ($\ell'' = \ell' - 2$) are strongly ordered as in $R[12\cdots\ell''] = R''$. Then the volume element in the last three variables in spherical coordinates is $r^2 dr d\Omega_2$, and so the integration region is effectively R'' but with $x_{\ell''}$ replaced by r. Since $\ell'' < \ell$, integrals in S will never lead to saturation.

Cut diagrams are easier to compute than uncut Feynman diagrams for three reasons. First and most trivial, a cut line contains a $\delta(sz)$ which makes the corresponding "$-$" integration simpler to carry out. Second and more importantly, the δ function demands the absence of the "$-$" momentum across this line, and so the cut line is cut also in the sense of being an open electric circuit. This generally reduces the number of possible flow diagrams and makes the corresponding integral easier to saturate. For example, each of the two-loop diagrams in Fig. 13 has only one flow path. Third, the flow pattern often leads to vanishing cut diagrams. For example, both diagrams 13(c) and 13(d) are zero from the "$+$" integration around the loop (12345) because the "$-$" flows around that loop are all in the same direction. This accounts for the equality $C17_c = C18_c = 0$ in Eq. (6.1).

The cost of this simplicity is the presence of tricky diagrams, which are cut diagrams that are apparently logarithmic divergent at large k_{a+}. This happens whenever there is a loop with only one arrow present. Arrows on the top fermion line should not be counted for this purpose because their approximate propagators $1/(sz + i\epsilon)$ no longer carry any k_{a+}. Figures 13(a) and 13(b) are examples of such diagrams. This apparent divergence is produced by the approximation of replacing the inverse propagators of an upper line by $sz + i\epsilon$, thus losing some q_+ factors needed for convergence. To regulate it we must replace the δ function of the cut line
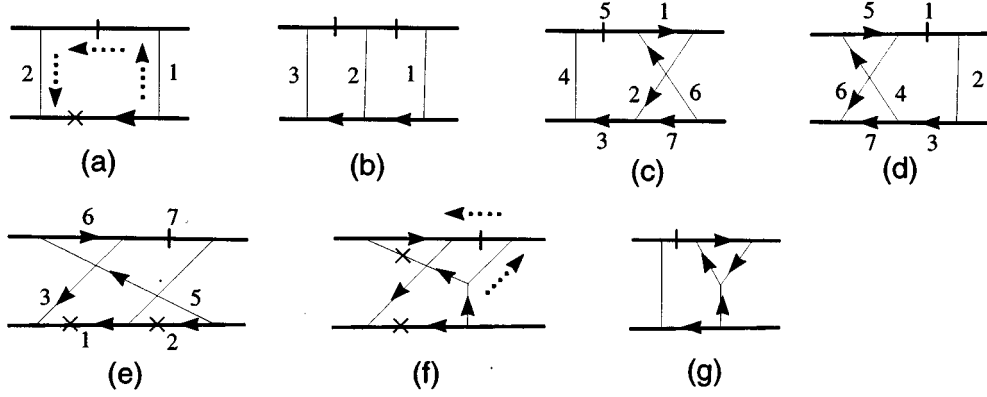
FIG. 13. Sample cut diagrams to illustrate their computation.

by a smeared δ function, thereby allowing a small amount of "$-$" momentum to flow through, and in the process restoring the lost q_+ factor. If we do so to Fig. 13(a), the k_+ integration is no longer divergent, it will have exactly the same flow path as in Fig. 12(a) and this is indicated in Fig. 13(a) by the dotted arrows; so a pole can be taken at the bottom fermion line as shown. The result is given by Eq. (B1) to be $\frac{1}{2}(g^4 i/2s)I_2$, the extra $\frac{1}{2}$ being there because the x integration is bounded by the flow path in Fig. 12(a) to be between 0 and 1, and so only half of the $\delta(sx)$ is integrated. When multiplied by the QED vertex and normalization factor $(2s)^2/(2m)^2$, one obtains $B1_c$ in Eqs. (6.1).

There is another way to compute Fig. 13(a). This is to recognize the fact that the cut makes it symmetric in lines 1 and 2, and so we may replace the diagram by half the sum of it and its crossed diagram. Using the sum rule (3.4), $a[12]+a[21]=a[1|2]$, a cut can be produced at the bottom line, and the resulting factor $-2\pi i\,\delta(\sqrt{s}q_{1+})$ makes the q_{1+} integration convergent. See Fig. 14. Moreover, the result of this "$+$" integration is $-2\pi i$, exactly the same as if we were to do it by residue calculus. The extra factor of $\frac{1}{2}$ obtained in the last paragraph now emerges because the double-cut diagram on the right of Fig. 14 is the sum of two diagrams.

Now we come to the tricky diagram 13(b), which unlike the one-loop case is much more difficult to compute by regu-

FIG. 14. One-loop tricky diagram and its computation.

lating the δ functions. The reason is that there are now two cut lines, the relative magnitude of the small "$-$" flows matters, and that produces once again two flow diagrams like Fig. 12(b) and 12(c). The poles are no longer at the bottom fermion line and the computation is no simpler than the uncut diagrams. We must then compute it by the second method. With the double cuts in Fig. 13(b), it is symmetric in all the q_{i-} variables. Insisting on this symmetry, Fig. 13(b) is equal to 1/3! times the sum of six diagrams, obtained by permuting the bottom gluon lines in all possible ways. From the factorization formula $a\{1;2;3\}=a[1|2|3]$ used on the bottom line, the result is equal to a diagram with all its fermion propagators cut. So Fig. 13(b) is given by Eq. (B1) to be $g^6(-2\pi i)^2 I_3/(4\pi s)^2 3! = -g^6 I_3/24s^2$. Incorporating the extra QED factor $-(2s)^3/(2m)^2$ for the $\mathcal{T}$ matrix, we obtain the contribution of $C15_c$ to $\mathcal{M}\equiv(2m^2/g^2)\mathcal{T}$ shown in Eqs. (6.1).

We conclude this appendix by discussing the remaining expressions in Eqs. (6.1)–(6.3). We shall use the notation $\langle B2_c\rangle$ to denote the spacetime contribution to $B2_c$, etc. Then $\langle B2_c\rangle=\langle B2\rangle, \langle C12_c'\rangle=\langle C_1 2_c''\rangle=\langle C12\rangle, \langle C16_c\rangle =\langle C16\rangle$, and $\langle C19_c\rangle=\langle C19\rangle$ can be obtained from Eqs. (2.1). The zero of $C19_c$ in Eqs. (6.1) is due to the vanishing of the color factor as shown in Fig. 11. Next, we compute $\langle C3_c'\rangle=\langle C3_c''\rangle$. The flow path of this is shown in Fig. 13(f), with the dotted arrows indicating the small regulating current which is allowed to flow only in the direction shown. The calculation is identical to the uncut diagram, [3] except that the factor $-\frac{1}{2}\ln^2 s$ is replaced by $\frac{1}{2}(\ln s)(-2\pi i)$ ($-2\pi i$ from the cut, $\ln s$ because only one uncut line is left on top, and $\frac{1}{2}$ because only half of the δ function is integrated). The result can then be read off from Eqs. (2.1) to be

$$\langle C3_c'\rangle=\langle C3_c''\rangle=-g^2\beta i(\ln s)\tfrac{1}{4}J_2 I_2, \qquad (B6)$$

which gives rise to the expression in Eqs. (6.3).

Finally, we must show that $C7_c'=0$ and $C7_c''{}^{=0}$. The former can be seen from the flow path in Fig. 13(g), where the arrows around the small triangle go around in a closed loop. The latter is so because the scalar diagram in Fig. 7 for $C7_c''$ is symmetrical in lines 2 and 3 but the triple gluon vertex is antisymmetrical in these two lines.

[1] ZEUS Collaboration, M. Derrick, Phys. Lett. B **315**, 481 (1993); **332**, 228 (1994); H1 Collaboration, T. Ahmed *et al.*, Nucl. Phys. **B429**, 477 (1994); Phys. Lett. B **348**, 681 (1995).

[2] F.E. Low, Phys. Rev. D **12**, 163 (1975); S. Nussinov, Phys. Rev. Lett. **34**, 1286 (1975).

[3] H. Cheng and T.T. Wu, *Expanding Protons: Scattering at High Energies* (M.I.T. Press, Cambridge, MA, 1987).

[4] N.T. Nieh and Y.P. Yao, Phys. Rev. Lett. **32**, 1074 (1974); Phys. Rev. D **13**, 1082 (1976); B. McCoy and T.T. Wu, Phys. Rev. Lett. **35**, 604 (1975); Phys. Rev. D **12**, 3257 (1975); **13**, 1076 (1976); L. Tyburski, *ibid.* **13**, 1107 (1976); L.L. Frankfurt and V.E. Sherman, Yad. Fiz. **23**, 1099 (1976) [Sov. J. Nucl. Phys. **23**, 581 (1976)]; A.L. Mason, Nucl. Phys. **B117**, 493 (1976).

[5] L.N. Lipatov, Yad. Fiz. **23**, 642 (1976) [Sov. J. Nucl. Phys. **23**, 338 (1976)]; Ya.Ya. Balitskii and L.N. Lipatov, *ibid.* **28**, 1597 (1978); **28**, 822 (1978).

[6] J. Bartels, Phys. Lett. **68B**, 258 (1977); Nucl. Phys. **B151**, 293 (1979); J.B. Bronzan and R.L. Sugar, Phys. Rev. D **17**, 585 (1978); V.N. Gribov, Zh. Éksp. Teor. Fiz. **53**, 654 (1967) [Sov. Phys. JETP **26**, 414 (1968)]; L.V. Gribov, E.M. Levin, and M.G. Ryskin, Phys. Rep. **100**, 1 (1983).

[7] C.Y. Lo and H. Cheng, Phys. Rev. D **13**, 1131 (1976); **15**, 2959 (1977); H. Cheng, J.A. Dickinson, and K. Olaussen, *ibid.* **23**, 534 (1981).

[8] E.A. Kuraev, L.N. Lipatov, and V.S. Fadin, Zh. Éksp. Teor. Fiz. **71**, 840 (1976) [Sov. Phys. JETP **44**, 443 (1976)]; **72**, 377 (1977); **45**, 199 (1977); J.A. Dickinson, Phys. Rev. **16**, 1863 (1977); L.N. Lipatov, in *Perturbative Quantum Chromody-namics*, edited by A.H. Mueller (World Scientific, Singapore, 1989).

[9] H. Cheng and T.T. Wu, Phys. Rev. Lett. **22**, 666 (1969).

[10] Y.J. Feng and C.S. Lam (unpublished).

[11] Note, however, that for later convenience the fermion arrows in Fig. 1 and all subsequent figures are drawn from right to left, reflecting the order one writes matrices as well as initial and final states on a piece of paper, whereas in Ref. [3] they are drawn in a more conventional way from left to right.

[12] There is a misprint in Fig. 12.7 of Ref. [3]. The $\mathbf{G}_2$ portion of diagram 16 should have a coefficient $3n/2$ rather than $n^2/2$.

[13] B.W. Lee and R.F. Sawyer, Phys. Rev. **127**, 2266 (1962); J.C. Polkinghorne, J. Math. Phys. **4**, 503 (1963); P.G. Federbush and M.T. Grisaru, Ann. Phys. (N.Y.) **22**, 263 (1963); **22**, 299 (1963); J.D. Bjorken and T.T. Wu, Phys. Rev. **130**, 2566 (1963); G. Tiktopoulos, *ibid.* **131**, 480 (1963); **131**, 2372 (1963); R.J. Eden, P.V. Landshoff, D.I. Olive, and J.C. Polkinghorne, *The Analytic S-Matrix* (Cambridge University Press, Cambridge, England, 1966); J.V. Greenman, J. Math. Phys. **7**, 1782 (1967); **8**, 26 (1967); C.S. Lam, Nuovo Cimento **62A**, 97 (1969).

[14] C.S. Lam and K.F. Liu, ''A multiple commutator formula for the sum of Feynman diagrams,'' Report No. McGill/96-12, hep-ph 9604337 (unpublished).

[15] H. Cheng and T.T. Wu, Phys. Rev. **186**, 1611 (1969); M. Levy and J. Sucher, *ibid.* **186**, 1656 (1969).

[16] C.Y. Lo, Nucl. Phys. **B157**, 212 (1979); Phys. Rev. D **23**, 508 (1981).